Very Efficient Tone Reservation PAPR Reduction Fully Compatible with ATSC 3.0 Standard: Performance and Practical Implementation Analysis

Naila Lahbabi, Sri Satish Krishna Chaitanya Bulusu, Jean-François Hélard, Matthieu Crussière

Very Efficient Tone Reservation PAPR Reduction Fully Compatible with ATSC 3.0 Standard: Performance and Practical Implementation Analysis

Naila Lahbabi†, S. S. Krishna Chaitanya Bulusu⋆, Jean-François Hélard† and Matthieu Crussière†
† Univ Rennes, INSA Rennes, CNRS, IETR-UMR6164, F-35000 Rennes, France.
⋆ Mahindra École Centrale, Survey No: 62/1A Bahadurpally, Hyderabad, India.
{naila.lahbabi, jean-francois.helard, matthieu.crussiere }@insa-rennes.fr.
{krishnachaitanya.bulusu@mechyd.ac.in.}

***Abstract*—A common issue in any multicarrier communication system such as the American digital video broadcasting (ATSC 3.0) standard is the high peaks of the transmitted signal. This disadvantage constrains the high power amplifiers to be deployed in their linear region which lowers their power efficiency. To overcome this issue, various techniques aiming at reducing the signal fluctuations have been investigated. Recently, Tone Reservation (TR) based algorithms have been studied and proposed for the second generation of Digital Video Broadcasting (DVB-T2) and ATSC 3.0 standards. The algorithm is essentially based on an iterative gradient approach to cancel one peak of the time-domain signal at each iteration. In this paper, we propose a novel TR-based algorithm implementable and compatible with the ATSC 3.0 standard and named as Grouped Carrier Peak Windowing (GCPW). This algorithm is based on a new kernel definition targeting the cancellation of multiple signal peaks at a time which highly reduces the total number of iterations, therefore reducing the system global latency and being more suited for implementation in today's ATSC 3.0 transmitters. Taking into account hardware resources requirements, we propose a new method to select the highest signal peaks to be considered in the PAPR reduction process. Hence, the system latency, complexity and memory resources are reduced and better performance than the ATSC 3.0 gradient-based algorithm can be offered. The implementation of the GCPW algorithm in fixed-point architectures is also studied and optimized in this paper. We demonstrate through simulation results that the proposed algorithm offers very good performance/latency/complexity/memory trade-off in both floating and fixed point implementations.**

***Index Terms*—OFDM, Broadcasting, Peak-to-average power ratio, Power control, ATSC 3.0, Non-linear HPA, Modulation error ratio, Tone reservation, computational complexity, kernel optimization, latency, fixed-point implementation, quantization.**

I. Introduction

ORTHOGONAL Frequency Division Multiplexing (OFDM) is a multicarrier modulation technology widely used in various systems such as Digital Video Broadcast (DVB) and Long Term Evolution (LTE) and was recently adopted by the American digital video broadcasting (ATSC 3.0) specifications. Like any multicarrier modulation, the transmitted OFDM signal is characterized by high peak values in the time-domain since many subcarrier components are added via the IFFT. As a result, OFDM systems are known to suffer from high Peak-to-Average-Power-Ratio (PAPR) which represents one of the most disadvantages of these systems.

High Power Amplifier (HPA) is an essential component in any modern communication system and it is inherently Non-Linear (NL). The HPA is more power efficient when operating near its NL region which leads to severe in-band and out-of-band distortions. When amplified by a NL HPA, high PAPR signals are more susceptible to amplitude and phase distortions, due to the non-linearity of the HPA conversion characteristics. To overcome this issue, the HPA can be operated in its linear region, leading to very poor power efficiency.

PAPR reduction techniques aim at decreasing the signal fluctuations in order to bring the HPA operating point near to the saturation region where its power efficiency is maximized. Several approaches that have been studied to mitigate the PAPR issue of OFDM systems are summarized in [1] [2] [3]. This problem has also been analyzed in the case of MIMO and multi-user systems, e.g. in [4]. Among the most widely known PAPR reduction techniques, clipping and filtering [5], coding [6], partial transmit sequence [7] and selected mapping [8]. Unfortunately, these PAPR methods suffer from low performance/complexity trade-off and the necessity, for some of them, to transmit side information which limits the gain of such techniques.

Alternatively, Tone Reservation (TR) [9] and Active Constellation Extension (ACE) [10] are two PAPR methods investigated recently and promising high potential without the necessity of side information transmission. These techniques have been adopted by different standards such as DVB-second generation (DVB-T2) [11], DVB for Next Generation Handled (DVB-NGH) and recently by the ATSC 3.0 standard [12].

TR concept was originally introduced by Tellado in [9] and consists in dedicating a subset of subcarriers called Peak Reserved Tones (PRT) to reduce the signal PAPR. The time-domain kernel obtained by loading complex values on these PRTs is added to the original signal leading to a new OFDM signal with lower PAPR. The main objective of TR concept is the computation of complex symbols assigned to the PRTs in order to lower the PAPR of the resulting signal. The optimal solution is originally presented as a convex optimization problem but can easily be transformed

to a linear problem. Thus, the computation of these complex values can be performed iteratively. In DVB-T2, DVB-NGH and ATSC 3.0, the TR concept is presented as an iterative gradient-based algorithm. At each iteration, the algorithm computes the highest peak of the time-domain signal and shifts a copy of the kernel to coincide with the peak position. Then, the kernel amplitude is scaled and its phase is adjusted in order to lower the detected peak of the resulting signal. The algorithm exits when the maximal number of iterations is reached or when all the signal peaks are below a predefined threshold V_{clip}. This TR algorithm is detailed in [11] for DVB-T2 and DVB-NGH standards and in [12] for the ATSC 3.0 standard. Unfortunately, this algorithm is complex and does not offer a sufficient performance/complexity trade-off to be implemented in todays modulators.

Recently, the TR concept has been investigated by different researchers. In [13], a solution based on genetic algorithms was proposed to search a sub-optimal set of PRT locations along with an adaptive amplitude clipping algorithm for TR-based PAPR techniques. A sub-optimal solution based on crossed entropy was proposed in [14] to search the sub-optimum amplitude and phase values of the PRTs configuration. In [15], the authors proposed a solution based on crossed entropy to find the optimal PRT set. An iterative algorithm was presented to search the optimal distribution of PRTs set taking into account the minimization of secondary kernel peaks in case of limited number of PRTs. A multi-stage TR-based PAPR reduction algorithm is proposed in [16]. It consists in using multi-stage TR schemes to process the OFDM signal. A two-stage example was presented where the OFDM signal peaks above a first threshold level are processed with the first TR block. Then, the processed signal is transmitted if its PAPR is below a second target threshold. Otherwise, the signal is processed with the second TR module. In [17], a novel TR algorithm based on the selection of a subcarrier having a phase close to ϕ, $\phi + \pi/2$, $\phi + \pi$ and $\phi - \pi/2$ is presented, where ϕ is the phase of the highest detected peak. In [18], a TR-based method is proposed to improve the convergence speed of clipping control methods. The authors proposed a Least Squares Approximation algorithm to generate the peak canceling signal by multiplying the filtered clipping noise by an optimized factor. The proposed algorithm offers the same PAPR reduction as clipping control methods with only two iterations. In [19], a TR-based algorithm is proposed to fit the peak canceling waveform to the filtered clipping noise. However, an additional IFFT is needed at every iteration along with an inversion operation of a matrix with a size equal to the square of number of PRTs. In [20], the authors presented a TR-based algorithm called Rotation Invariant Subcarrier Mapping to be used in DVB-T2 standard and offering similar performance as the DVB-T2 TR method. The algorithm consists in using the PRTs for PAPR reduction as well as for carrying information or signaling data. In [21], the authors proposed a TR algorithm based on sphere encoding with power constraint to search the optimal PAPR reducing signal.

Lately, a modified TR algorithm was proposed in [22]. It consists in modifying the TR structure by decomposing the OFDM symbol into a mixture of shorter symbols with less subcarriers. In [23], the authors proposed a modified Signal-To-Clipping TR algorithm for OFDM systems. To approximate the noise clipping signal, they proposed a Least Squares Approximation scheme to find the optimal factor multiplying the canceling signal so as to increase the convergence speed. With the same aim, [24] describes a parallelized version of the original TR algorithm. On the other hand, authors in [25] introduce an iterative algorithm trying to solve the QCQP problem at less complexity expense. However, all those proposed PAPR reduction techniques either remain too complex or offer reduced PAPR gain.

In [26] a promising TR-based algorithm named as Grouped Individual Carrier for Multiple Peaks (GICMP) was proposed for DVB-T2 standard. The main idea consists in a new definition of the peak canceling signal. In fact, the authors defined a new kernel by activating a sub-group of PRTs at each iteration. Instead of the pulse-like kernel defined by the DVB-T2 standard algorithm, they proposed a comb-like kernel which targets the reduction of multiple signal peaks at each iteration. Compared to the standard algorithm, GICMP offers very good performance with reduced complexity and is implementable and compatible with the DVB-T2 standard.

GICMP algorithm requires storage of all signal time-domain samples in addition to a sorting operation to detect the signal peaks. In this paper, we propose a novel TR-based algorithm implementable and compatible with ATSC 3.0 standard and named as Grouped Carrier Peak Windowing (GCPW). The proposed algorithm defines a new method to detect the signal peaks in order to reduce hardware resources such as latency, memory and complexity. Indeed, only signal peaks above a predefined and optimized threshold are targeted by GCPW algorithm. Hence, the OFDM time-domain samples can be processed when they are received without the necessity of storage and sorting operations as with GICMP algorithm. The simulation results show that the proposed implementation-friendly GCPW algorithm offers very good performance with less complexity and implementation resources requirements. Moreover, the GCPW algorithm is evaluated in fixed-point implementation and some minor modifications are proposed to reduce the quantization effects.

To sum up, this paper presents an in-depth study of the very efficient PAPR reduction GCPW algorithm for ATSC 3.0 standard taking into account all the practical issues related to the implementation. More precisely, this novel solution is optimized for high modes such as 8K and 32K modes which are the preferred modes for mobile and fixed reception, respectively.

The rest of this paper is organized as follows: Section II reminds the OFDM system model and some issues related to PAPR reduction. In Section III, we present the state of the art of TR solutions. In Section IV, the GCPW algorithm is described and the threshold computation is detailed. Section V deals with the implementation aspects of the proposed algorithm and gives an overview of fixed-point implementation and quantization. In Section VI, the threshold is optimized via simulations and the GCPW performance

in terms of Modulation Error Rate (MER) is compared to the GICMP performance and to those of the optimal and standard TR algorithms. In addition, the quantization impact on GCPW performance is also evaluated. Conclusions are drawn in Section VII.

II. Overview of OFDM system model and PAPR issues

A. OFDM System Model

Considering an OFDM system, the continuous-time baseband signal transmitted over N subcarriers can be expressed as

$$x(t) = \mathcal{F}\{\mathbf{X}\} = \frac{1}{\sqrt{N}} \sum_{k=0}^{N-1} X_k e^{j2\pi \frac{kt}{NT}}, 0 \leq t < NT, \quad (1)$$

where $\mathbf{X}$ is a sequence of complex symbols $[X_0, \ldots, X_n, \ldots, X_{N-1}]$, $T_s = NT$ is the OFDM symbol duration with T the sampling period. $\mathcal{F}$ is the OFDM modulation function and $j = \sqrt{-1}$.

B. HPA Model

In this paper, we consider the well-known Rapp model [27], commonly used to model solid-state HPAs in broadcasting systems. The equivalent continuous-time baseband output is given as

$$y(t) = \frac{x(t)}{\sqrt[2p]{1 + \left(\frac{|x(t)|}{v_{sat}}\right)^{2p}}}, \quad (2)$$

where $x(t)$ is the input signal, v_{sat} is the saturation voltage of the HPA and p is the knee factor which reveals the smoothness of transition from the linear region to the saturation region of the HPA.

In order to achieve undistorted amplified signal $y(t)$, the input power must be reduced by a value called the Input Back-Off (IBO) of the HPA. It represents the difference in dB between the input signal power at the operating point and at the saturation point, as given below

$$\text{IBO} = 10.\log_{10}\left(\frac{v_{sat}^2}{\mathbb{E}\left[|x(t)|^2\right]}\right), \quad (3)$$

where $\mathbb{E}[.]$ is the expectation operator.

C. PAPR Analysis

1) PAPR definition: It is well known that multicarrier signals may have very high peak values in the time-domain since many subcarrier components are added via the IFFT. The PAPR of $x(t)$ measures the ratio of the signal maximum instantaneous power to its mean power over a symbol period T_s, and is defined by

$$PAPR_{x(t)} = \frac{\|x(t)\|_\infty^2}{\mathbb{E}[\|x(t)\|_2^2]}, \quad (4)$$

where $\|.\|_\infty$ and $\|.\|_2$ denote $\mathcal{L}_\infty$ and $\mathcal{L}_2$ norms, respectively.

2) CCDF metric: In literature, the most common parameter considered to analyze the PAPR is the Complementary Cumulative Density Function (CCDF). It provides the probability of the signal exceeding a certain threshold γ (in dB), and is defined as [28]

$$CCDF_{x(t)}(\gamma) = \Pr(PAPR_{x(t)} > \gamma), \quad (5)$$

where $\Pr(.)$ denotes the probability function. The CCDF of PAPR computes only the probability that at least one sample, within the observation window, exceeds the given threshold. This parameter gives no statistics about the number of high peaks within the observation window that are more likely to undergo severe distortions. Thus, the NL effects of the PA on the signal can not be merely predicted via the CCDF metric. In fact, it is more interesting to measure how many peaks above a certain threshold, within the observation window, are susceptible to be distorted.

3) MER metric: Although the CCDF of PAPR is well-known in literature, the MER is the most widely used figure of merit for system performance in the broadcasting community and is defined in dB as

$$MER\{\mathbf{X}, \widehat{\mathbf{X}}\} = 10\log_{10}\left(\frac{\|\mathbf{X}\|_2^2}{\left\|\mathbf{X} - \widehat{\mathbf{X}}\right\|_2^2}\right), \quad (6)$$

where $\mathbf{X}$ is the ideal symbol vector measured at the input of the amplifier and $\widehat{\mathbf{X}}$ is measured at the output of the HPA. The denominator in (Eq. 6) presents the energy of the distortion which is related in time-domain to the energy above a given threshold. Unlike CCDF of PAPR, MER do not solely depend on the amplitude of the highest peak but mainly on the energy of the time-domain OFDM signal above this given threshold. Hence, MER reveals the distortion of the constellation points induced by the NL effects of the HPA and is very useful for the good dimensioning of the signal. Therefore, we consider in this paper MER as the metric for PAPR analysis.

III. Tone reservation based algorithms for PAPR reduction

A. TR Concept

The TR concept introduced by Tellado in [9] relies on the dedication of a subset of PRTs for PAPR reduction purposes. This subset of subcarriers is used to generate a kernel signal in the time-domain, which is then added to the original one in order to lower its PAPR. To better understand the difficulty behind practical TR principles implementation, let us consider that we allocate R tones for PAPR reduction of the OFDM system of N subcarriers. We define $\mathcal{B}$ as the PRT subset of these R locations and $\mathbf{C}$ as the vector of R peak reduction symbols transmitted on these positions and zeros elsewhere. Similarly, let the complement set $\mathcal{B}^c$ be the Data Tone (DT) subset of the useful data positions and $\mathbf{D}$ the vector of the $N-R$ associated transmitted data symbols and zeros elsewhere. The DT and PRT sets are totally disjoint, i.e. $\mathcal{B} \cap \mathcal{B}^c = \emptyset$. At the receiver side, only data tones are considered to recover the transmitted data. Hence, no side information is needed

in TR concept. The resulting signal to be transmitted can be represented in frequency and time domains as

$$\mathbf{X} = \mathbf{C} + \mathbf{D} \qquad \overset{\mathcal{F}}{\Longleftrightarrow} \qquad \mathbf{x} = \mathbf{c} + \mathbf{d}, \tag{7}$$

where

$$\mathbf{C} = \begin{cases} C_k \neq 0, & \forall k \in \mathcal{B}, \\ C_k = 0, & \forall k \in \mathcal{B}^c, \end{cases}$$

and

$$\mathbf{D} = \begin{cases} D_k \neq 0, & \forall k \in \mathcal{B}^c, \\ D_k = 0, & \forall k \in \mathcal{B}. \end{cases}$$

From this signal model, the PAPR of the baseband signal $\mathbf{x}$, defined over an observation window corresponding to the OFDM symbol size, is then defined as follows,

$$PAPR_x = \frac{\|\mathbf{x}\|_\infty^2}{\frac{1}{N}\|\mathbf{x}\|_2^2} = N\frac{\|\mathbf{c}+\mathbf{d}\|_\infty^2}{\|\mathbf{c}\|_2^2 + \|\mathbf{d}\|_2^2}. \tag{8}$$

From Eqs. (7) and (8), we understand that the central issue of TR concept is the design of efficient algorithms able to compute, for each new symbol, the adequate $\mathbf{c}$ (or equivalently the adequate complex values C_k to load on the reserved tones) so as to efficiently reduce the PAPR.

B. Theoretical Optimization Problem

It is possible to formulate the TR optimization problem as a Quadratically Constrained Quadratic Program (QCQP) [29]

$$\begin{aligned} \mathcal{P}_0 : \qquad & \min_{\mathbf{C}} \quad \Lambda = \left\|\mathbf{d} + \mathbf{F}_N^H \mathbf{C}\right\|_\infty^2 \\ & \text{subject to,} \quad \|\mathbf{C}\|_\infty^2 \leq \tfrac{\Gamma}{N-R}\,\|\mathbf{D}\|_2^2, \end{aligned}$$

where $\mathbf{F}_N$ is the Fourier matrix of size N and $\Gamma = 10^{\frac{\lambda}{10}}$ is the power level gap with λ the difference in dB between the maximum PRT power and the mean DT power. This problem essentially finds the optimal vector $\mathbf{C}$ of complex values to associate to the PRTs so as to minimize the maximum peak value Λ of the output signal. Note that the power constraint imposed on the reserved tones is a peak power constraint defined with respect to the power level associated to data tones. This corresponds to the case of DVB-T2, DVB-NGH and ATSC3.0 specifications, where $\lambda = 10$ dB maximum.

Problem $\mathcal{P}_0$ can also be viewed as a special case of Second Order Cone Program (SOCP) [30], which is a convex optimization problem class that minimizes a linear function over the intersection of an affine set and the product of second-order (quadratic) cones. Finding the optimal solution to $\mathcal{P}_0$ using SOCP or QCQP requires very high computational complexity which completely prevents the implementation of such algorithms in practical transmitters.

C. TR Gradient-Based Solutions

1) TR algorithm for ATSC 3.0 standard: The computation of the complex values C_k assigned to the reserved tones can be performed iteratively. For instance, the ATSC 3.0 broadcasting specifications include a gradient-based iterative algorithm for PAPR reduction. This solution, initially proposed in [31] and illustrated in Fig. 1 is based upon iteratively cancelling out the signal peaks by a set of impulse-like kernels. The reference kernel signal denoted as $\boldsymbol{\kappa}$, is a Dirac-like pulse obtained by letting $C_k = 1,\ \forall k \in \mathcal{B}$, that is

$$\boldsymbol{\kappa} = \mathcal{F}\{\mathbf{1}_{TR}\}, \quad \text{where, } \mathbf{1}_{TR} = \begin{cases} 1, & k \in \mathcal{B}, \\ 0, & k \in \mathcal{B}^c. \end{cases} \tag{9}$$

Based on this kernel definition, each peak of the time-domain signal can be mitigated or even cancelled by adequately shifting the original kernel $\boldsymbol{\kappa}$ to make its peak position coincide with the detected one. Then, the shifted kernel is scaled and subtracted from the original signal to reduce its peak amplitude. Hence, the QCQP optimization problem can be restated as follows

$$\begin{aligned} \mathcal{P}_1 : \min_{\rho_i,\ \tau_i} \quad & \Lambda = \left\|\mathbf{d} + \boldsymbol{\kappa} \circledast \textstyle\sum_{i=1}^{N_i} \rho_i \boldsymbol{\delta}_N[n-\tau_i]\right\|_\infty^2 \\ \text{subject to,} \quad & \|\mathbf{C}\|_\infty^2 \leq \tfrac{\Gamma}{N-R}\,\|\mathbf{D}\|_2^2, \end{aligned}$$

in which $\circledast$ stands for circular convolution and $\boldsymbol{\delta}_N[n]$ is the Dirac delta discrete sequence vector of size N. In $\mathcal{P}_1$, the search of the optimal solution translates into finding the optimal time delays τ_i and weigthing factors ρ_i, for a sufficient number of iterations N_i. The optimal resolution of $\mathcal{P}_1$ leads to the same final solution as solving $\mathcal{P}_0$. However, a suboptimal approach can be followed, by fixing Λ to a fixed reference value $\tilde{\Lambda}$ corresponding to the average value obtained in simulation by running the optimal solution. Then, an iterative process can be established consisting in detecting and cancelling the first highest peak, and then repeating the process iteratively for the other peaks. This iterative algorithm is schematically represented in Fig. 1. The algorithm exits as soon as the power constraint is violated or when a predefined maximum number of iterations is reached.

As shown later on and published in [32] [33], the gradient-based TR algorithm does not offer a sufficient performance-complexity trade-off to be implemented in today's DVB-T2 or ATSC 3.0 modulators. The major issue of this algorithm is its very slow convergence yielding a high number of iterations. A second issue is that it is inefficient in properly exploiting the available amount of power dedicated to the reserved tones. That is why, multiple researches have been focusing these last years on enhancing the performance of TR gradient-based algorithms (e.g. [35], [36]). However, even if some improvements have been achieved, the proposed solutions does not sufficiently alleviate the convergence and power constraint issues for practical implementation.

2) Time domain tracking power control: The power allocated to the PAPR reduction tones is limited by a predefined power constraint. The last version of the DVB-T2 standard [37] and the ATSC 3.0 standard [12] specify a Power Control (PC) scheme that controls at each iteration the power allocated to the PRTs. This PC scheme is referred to as *Time-domain Tracking PC* (TTPC) or DVB-T2 TR algorithm and is illustrated in Fig. 1. It defines an amplitude scaling factor α_k that is applied to the kernel $\boldsymbol{\kappa}$ at the i^{th} iteration such that the k^{th} PRT C_k, for $k \in \mathcal{B}$ exceeding the power limit is computed as follows

$$\alpha_k^{(i)} = \sqrt{\left(A_{max}\right)^2 - Im\{u_k^* r_k^{(i-1)}\}^2} + Re\{u_k^* r_k^{(i-1)}\}, \tag{10}$$

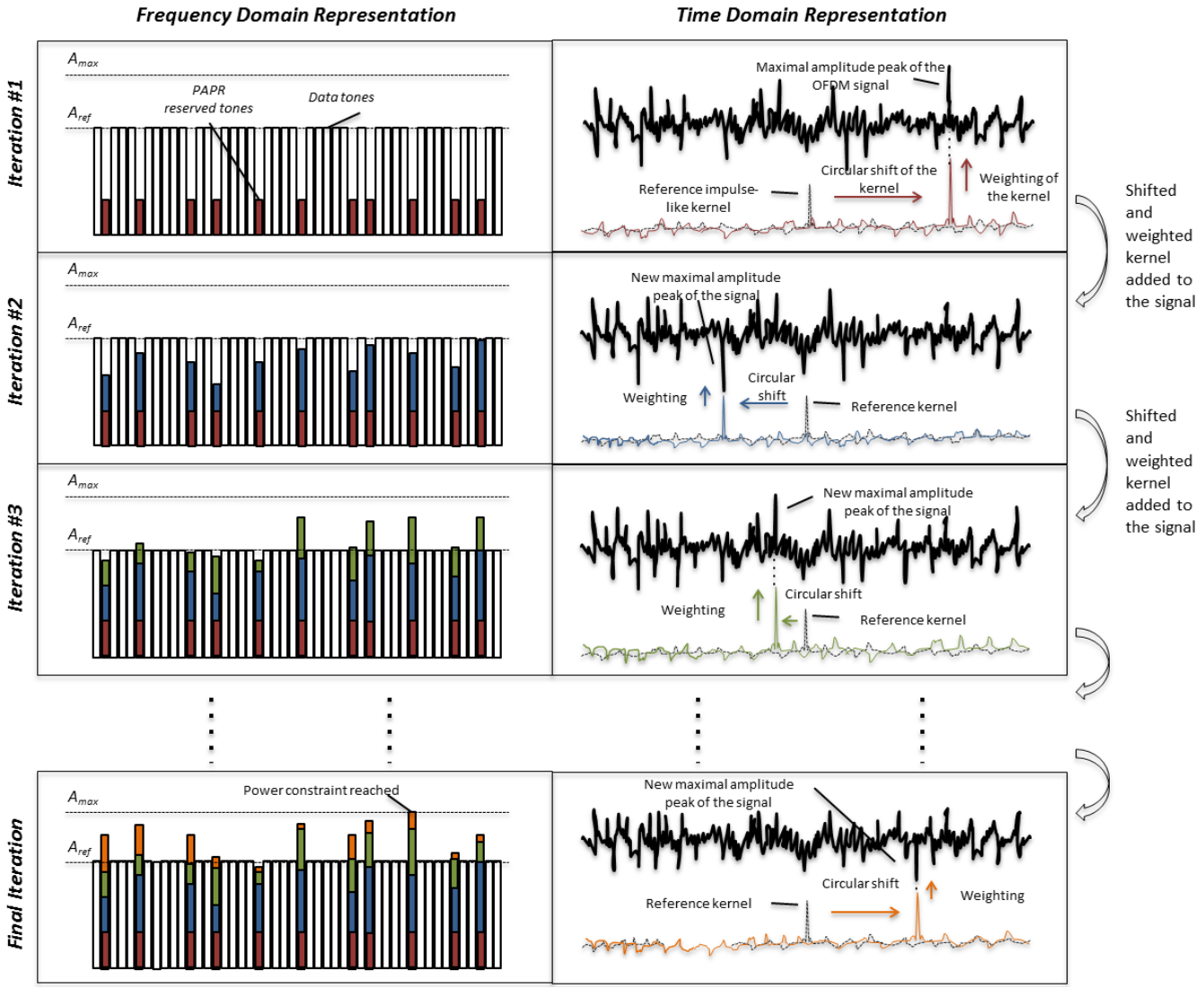

Fig. 1: Schematic representation of the TR gradient-based algorithm.

where,

- $u_k = \frac{1}{c[0]} e^{-\jmath 2\pi \left(\left(\mathcal{B}(k) - p_k \right) \mod N \right)} . e^{-\jmath \phi}$
- $c[0]$ is the peak of kernel $\boldsymbol{\kappa}$ at position 0,
- p_k is the position of the peak being processed,
- ϕ is the phase of the peak being processed,
- A_{max} is square root of the maximum power per PRT,
- $r_k^{(i-1)}$ is the value of C_k after the previous iteration.

The TTPC algorithm aims at finding α_k for every PRT, in such a way that the resulting amplitude of the sum of the build-up PRT and current PRT is equal to $A_{max} = \sqrt{P_{max}}$. Without violating the PC, the amount of the allowed scaling is given by

$$\alpha = \min_{k \in \mathbf{B}} \left(\alpha_k^{(i)} \right) \tag{11}$$

Fig. 1 shows the power build up after each iteration. The TTPC algorithm exits when at least one of the PRTs reaches the allowed power limit.

3) TR guidelines in ATSC 3.0: We denote κ as the percentage of the subcarriers dedicated for PAPR reduction. For example, in ATSC 3.0 standard [12], $\kappa = 1$, i.e. 1 %. The number of reserved tones for PAPR reduction for different OFDM symbol sizes is given in Table I.

TABLE I: Size of R for different modes in ATSC 3.0.

MODE	8K	16K	32K
N	8192	16384	32768
R	72	144	288

In ATSC 3.0, the number of active subcarriers denoted by NoC is given by the following expression

$$NoC = NoC_{max} - C_{red-coeff} \times C_{unit}, \tag{12}$$

where NoC_{max} is the maximum number of subcarriers in a symbol and C_{unit} is a control unit factor taking a value of 96 and 384 for 8K and 32K modes, respectively. $C_{red-coeff}$ is a positive integer ranging from 0 to 4 and indicating the number of carriers to be reduced.

IV. New Kernel definition for TR-based PAPR reduction algorithms

In this section, we introduce a new kernel definition and power allocation to the PRTs to benefit from all the amount of power available for PAPR reduction. We present a first algorithm referred to as Grouped Individual Carrier allocation for Multiple Peaks reduction (GICMP) which offers a good performance/complexity trade-off [26]. Then, we propose an implementation-friendly algorithm named as Grouped Carrier Peak Windowing (GCPW) in order to reduce the hardware resource requirements of the previous one.

The GICMP algorithm is based on a grouping strategy of the PRTs. More precisely, the reserved tones are divided into G groups as follows

$$\mathcal{B} = \{\mathcal{B}_1, \ldots, \mathcal{B}_G\}, \tag{13}$$

with,

$$\mathcal{B}_i = \big\{\mathcal{P}_{i,j}, \quad 1 \leq i \leq G, \quad 1 + \frac{(i-1)R}{G} \leq j \leq 1 + \frac{iR}{G}\big\}, \tag{14}$$

where $\mathcal{P}_{i,j}$ is the j^{th} tone in $\mathcal{B}_i$. Instead of a Dirac-type kernel as suggested by the DVB-T2 and the ATSC 3.0 specifications, a comb-like kernel obtained by activating a group of reserved tones is generated at each iteration of the algorithm. Hence, the total number of iterations equals the number of PRT groups denoted here by G. At each iteration i, the proposed kernel is then defined as

$$\boldsymbol{\upsilon}_i = \mathcal{F}\left\{\mathcal{B}_i\right\}, \tag{15}$$

with,

$$\mathcal{B}_i = \begin{cases} \mathcal{P}_{i,j} = 1, & 1 + \frac{(i-1)R}{G} \leq j \leq 1 + \frac{iR}{G} \\ \mathcal{P}_{i,j} = 0, & otherwise. \end{cases}$$

The reason for such a choice is threefold. At first, allocating each group of tones one by one allows to perfectly and implicitly control the PRTs power. Then, the comb-like structure of the time-domain kernel is expected to be able to reduce multiple peaks at a time since its energy is spread all over the OFDM symbol duration. The condition for that is to compute the adequate phase-shift of the kernel as detailed hereafter. Last but not least, the kernel computation can directly be processed in time domain, without the use of any additional IFFT, since it is easily computed as follows

$$\upsilon_i(n) = \sum_{j=1}^{\frac{R}{G}} p_{i,j}(n), \qquad 1 \leq i \leq G, \tag{16}$$

where,

$$p_{i,j}(n) = \frac{1}{N} e^{-\jmath \frac{2\pi \mathcal{P}_{i,j} n}{N}}, \qquad 0 \leq n < N, \tag{17}$$

is the kernel associated to the $\mathcal{P}_{i,j}$ PRT.

A. Optimization Problem Formulation

From this new kernel definition, we can state the modified optimization problem $\mathcal{P}_2$ as follows

$$\mathcal{P}_2 : \quad \min_{\rho_{i,j},\ \phi_{i,j}} \quad \left\| \mathbf{d} + \sum_{i=1}^{G} \sum_{j=1}^{\frac{R}{G}} \rho_{i,j} e^{-\jmath\phi_{i,j}} \boldsymbol{p}_{i,j} \right\|_{\infty}^{2}, \quad \text{subject to,} \quad \rho_{i,j} \leq \tfrac{\Gamma}{N-R} \left\|\mathbf{D}\right\|_2^2.$$

It becomes obvious that the power constraint is easily controlled via $\rho_{i,j}$. Optimal resolution of problem $\mathcal{P}_2$ involves an intensive search of the optimal values $\rho_{i,j}$ and $\phi_{i,j}$. However, after thorough analysis of the optimal values obtained in simulations by running the original QCQP algorithm on $\mathcal{P}_0$, it turns out that almost all reserved tones should be loaded at the maximum allowed power level A_{max}. Hence, a simplified sub-optimal problem can be obtained by fixing $\rho_{i,j} = A_{max},\ \forall i, j$. Also, the search of the optimal $\phi_{i,j}$ values can be simplified by converting the infinite norm into a quadratic one, but restricting the computation upon a given subset of time samples corresponding to the highest peak values of the OFDM time-domain signal. Hence, instead of minimizing the maximum peak amplitude (infinite norm criterion), we rather minimize the energy carried by a set $\mathcal{S}$ of multiple highest peaks. The corresponding optimization problem we have thus proposed states as

$$\mathcal{P}_3 : \min_{\phi_{i,j}} \quad \left\| \mathbf{d}(\mathcal{S}) + \sum_{i=1}^{G} \sum_{j=1}^{\frac{R}{G}} A_{max} e^{-\jmath\phi_{i,j}} \boldsymbol{p}_{i,j}(\mathcal{S}) \right\|_2^2, \tag{18}$$

where $\mathbf{d}(\mathcal{S})$ and $\boldsymbol{p}_{i,j}(\mathcal{S})$ are the data signal and kernel time samples at the highest peak positions given by index set $\mathcal{S}$.

B. GICMP Algorithm

The crucial step in the resolution of Problem $\mathcal{P}_3$ is the computation of the optimal phase $\phi_{i,j}$ for each comb-like kernel $\boldsymbol{p}_{i,j}$, taking into account several peak positions (hence the algorithm name). As in the gradient-based case, a sub-optimal solution is used to solve the problem iteratively, i.e. via parallel computation of the optimal phases $\phi_{i,j}$. For one particular iteration i, assuming a set $\mathcal{S}$ of highest peaks of the signal and a kernel $\boldsymbol{p}_{i,j}$ the optimal phase $\phi_{i,j}^*$ is obtained by solving the following sub-problem

$$\mathcal{SP}_3 : \quad \min_{\phi_{i,j}} \ \left\| \mathbf{d}(\mathcal{S}) + \boldsymbol{p}_{i,j}(\mathcal{S}).A_{max} e^{-\jmath\phi_{i,j}} \right\|_2^2. \tag{19}$$

Such a sub-problem involves a differential quadratic form which is easy to minimize. After classical mathematical manipulations, the optimal phase $\phi_{i,j}^*(\mathcal{S})$ can then be expressed as

$$\phi_{i,j}^*(\mathcal{S}) = \text{atan}\left(\frac{\mathfrak{Im}\left\{\mathbf{d}^{\mathcal{H}}(\mathcal{S}) \boldsymbol{p}_{i,j}(\mathcal{S})\right\}}{\mathfrak{Re}\left\{\mathbf{d}^{\mathcal{H}}(\mathcal{S}) \boldsymbol{p}_{i,j}(\mathcal{S})\right\}} \right) - \frac{\pi}{2}. \tag{20}$$

Eventually, the GICMP algorithm is illustrated in Fig. 2 where each group of PRTs is composed of two tones. At every iteration i, $S = \text{Card}\{\mathcal{S}\}$ highest signal peaks are detected and then the optimal phases $\phi_{i,1}^*$ and $\phi_{i,2}^*$ are computed for both tones. The resulting kernel is then used to reduce the detected peaks.

From an initial time-domain OFDM symbol vector $\mathbf{d}$, the GICMP TR-based PAPR reduction algorithm applied on R reserved tones yields the following symbol vector :

$$\mathbf{x} = \mathbf{d} + \mathbf{c} \qquad \text{with, } \mathbf{c} = A_{\max} \sum_{i=1}^{G} \sum_{j=1}^{\frac{R}{G}} \boldsymbol{p}_{i,j} e^{-\jmath \phi^*_{i,j}(\mathcal{S})}, \quad (21)$$

where $\boldsymbol{p}_{i,j}$ is obtained from (17) and $\phi^*_{i,j}(\mathcal{S})$ is iteratively computed from (20).

In [34], an algorithm named as Individual Carrier Multiple Peaks (ICMP) has been presented. Similarly to the GICMP algorithm, the ICMP is also based on a comb-like kernel definition. However, the generated kernel is associated to the activation of a single PRT per iteration to cancel multiple signal peaks. The ICMP algorithm is carried out in the same way. The main difference is the total number of iterations which is no longer equal to the number of PRT groups but to the number of available PRTs. Since DVB-T2 and ATSC3.0 standards reserve 1% of the subcarriers for PAPR reduction, this would lead to a number of iterations raising from $R = 9$ in 2K mode to $R = 288$ in 32K mode. Since the latter mode is most likely to be deployed for terrestrial broadcast networks, ICMP is not yet suited to such a situation. On the other hand, the proposed GICMP algorithm executes multiple peaks search per group of PRTs which lowers the total number of iterations. Hence, the latency, which is essentially driven by the peaks search process, can be substantially lowered since it becomes proportional to the number of groups.

C. GCPW Algorithm

The global latency is the most important criterion in any PAPR reduction algorithm. With the GICMP algorithm, it is mainly related to the number of iterations which equals the number of PRT groups. Additionally, the GICMP latency depends on the search of the S highest peaks performed at each iteration. Indeed, this operation requires the processing of the whole OFDM signal, meaning that the time-domain signal values should be first sorted and then the S highest peaks are selected and stored. To further improve the GICMP latency, we propose a new TR-based algorithm named GCPW. The search of the S highest peaks can be simplified by selecting, at each iteration i, the first subset $\mathcal{S}_i$ of signal peaks above a given threshold $\tilde{\lambda}$. As in the gradient-based algorithm, such threshold can be optimized and pre-calculated through simulations. In addition, to limit the size of storage of these peaks, only $\text{Card}\{\mathcal{S}_i\} \leq S$ peaks are kept for the phase computation, where S is the maximum number of peaks. In this case, the sub-optimal problem $\mathcal{SP}_3$ is restated as follows

$$\begin{aligned} \mathcal{SP}_4 : \quad & \min_{\phi_{i,j}} \left\| \mathbf{d}(\mathcal{S}_i) + \mathbf{p}_{i,j}(\mathcal{S}_i).A_{max} e^{-\jmath \phi_{i,j}} \right\|_2^2, \\ \text{subject to,} \quad & \mathcal{S}_i = \left\{ k \ : \ \left| d(k) + \textstyle\sum_{j=1}^{i-1} c^j(k) \right| \ > \ \tilde{\lambda} \right\}, \\ \text{with,} \quad & S_i = \text{Card}\{\mathcal{S}_i\} \leq S, \end{aligned}$$

where $\mathcal{S}_i$ is the instantaneous subset of time-domain peak samples considered at each iteration, $c^j(k)$ is the kernel samples at iteration j and $\tilde{\lambda}$ an amplitude threshold optimized through simulations as in the gradient-based case.
Consequently, the optimal phase solution is expressed as

$$\phi^*_{i,j}(\mathcal{S}_i) = \text{atan}\left(\frac{\mathfrak{Im}\left\{ \mathbf{d}^{\mathcal{H}}(\mathcal{S}_i) \boldsymbol{p}_{i,j}(\mathcal{S}_i) \right\}}{\mathfrak{Re}\left\{ \mathbf{d}^{\mathcal{H}}(\mathcal{S}_i) \boldsymbol{p}_{i,j}(\mathcal{S}_i) \right\}} \right) - \frac{\pi}{2}, \quad (22)$$

Threshold computation: The threshold $\tilde{\lambda}$ is calculated based on the mean value of the OFDM signal over M symbols as

$$A_{mean} = \frac{1}{M.N} \sum_{m=1}^{M} \sum_{n=1}^{N} \left| d_m(n) \right|, \quad (23)$$

where $|d_m(n)|$ are the absolute values of all time samples of the m^{th} symbol. The threshold is then expressed as

$$\tilde{\lambda} = \beta . A_{mean}, \ \beta \in \mathbb{R}_+, \quad (24)$$

with β a positive multiplicative factor.

To sum up, GCPW has two additional constraints related to the threshold $\tilde{\lambda}$ and to the number of peaks S which leads to some performance degradation compared to the GICMP algorithm. To maximize the MER, the number of groups and the threshold value should be optimized. As $\tilde{\lambda}$ defines the number of targeted peaks, this value should be wisely optimized in order to select the most significant peaks. As the optimal value of $\tilde{\lambda}$ is fixed for each OFDM mode, it can be pre-computed and stored in any digital platform. Consequently, the threshold based approach of the proposed GCPW algorithm highly reduces the complexity issue identified with GICMP.

V. Implementation Aspects of GCPW algorithm

The gain in performance of any TR-based algorithm has come at a cost of substantial increase in computation and memory storage resources. Fixed-point implementation has the potential to alleviate some of these complexities and facilitate potential deployment on embedded hardware, albeit, with some performance degradation due to quantization error.

A. Block Diagram of GCPW Algorithm

The block diagram of the GCPW algorithm is illustrated in Fig. 3. At the IFFT block output, the signal is stored and updated at each iteration. During the peak search process, the GICMP algorithm needs storage of absolute values of all N signal samples. Then, these values are sorted and the S highest peaks and their positions, denoted here by *maxVal* and *maxPos*, are detected and stored by the *Detect Max* module.

On the other hand, GCPW is an implementation-friendly algorithm proposed to avoid the tedious peak search and sorting operation. The GCPW performs a peak windowing search where only maximum S peaks above the predefined threshold $\tilde{\lambda}$ are targeted. At every iteration i, the first $S_i \leq S$ peaks above $\tilde{\lambda}$ are stored and no sorting operation is required. Hence, GCPW has lower processing delay than GICMP since the OFDM time samples can be processed as and when they are received. After the peak selection process, the GCPW algorithm computations are carried out by the blocks illustrated by the the red dashed boxes in Fig. 3: Kernel, A, B, Angle and New kernel.

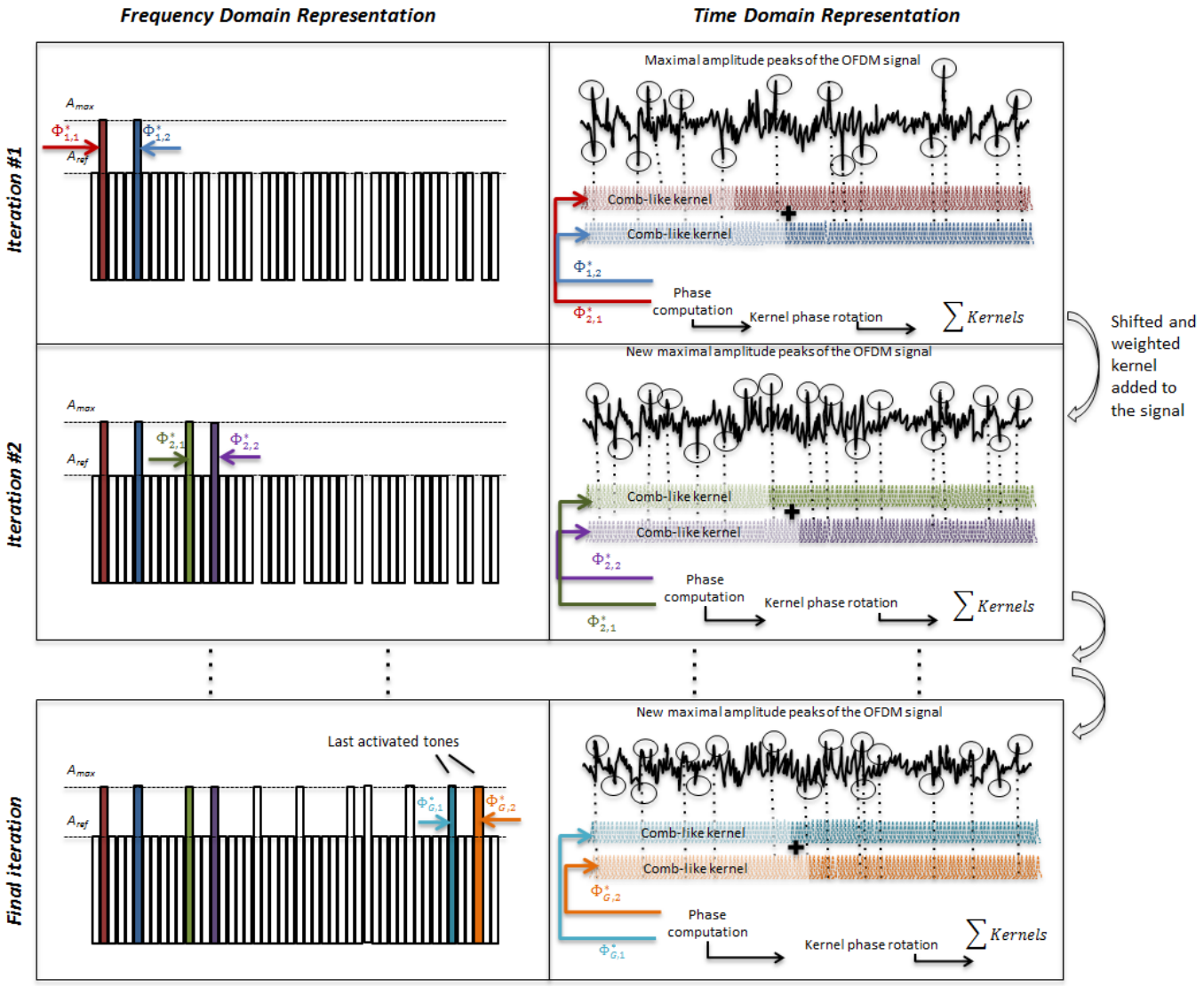

Fig. 2: Iterative power allocation of the PRTs with GICMP algorithm.

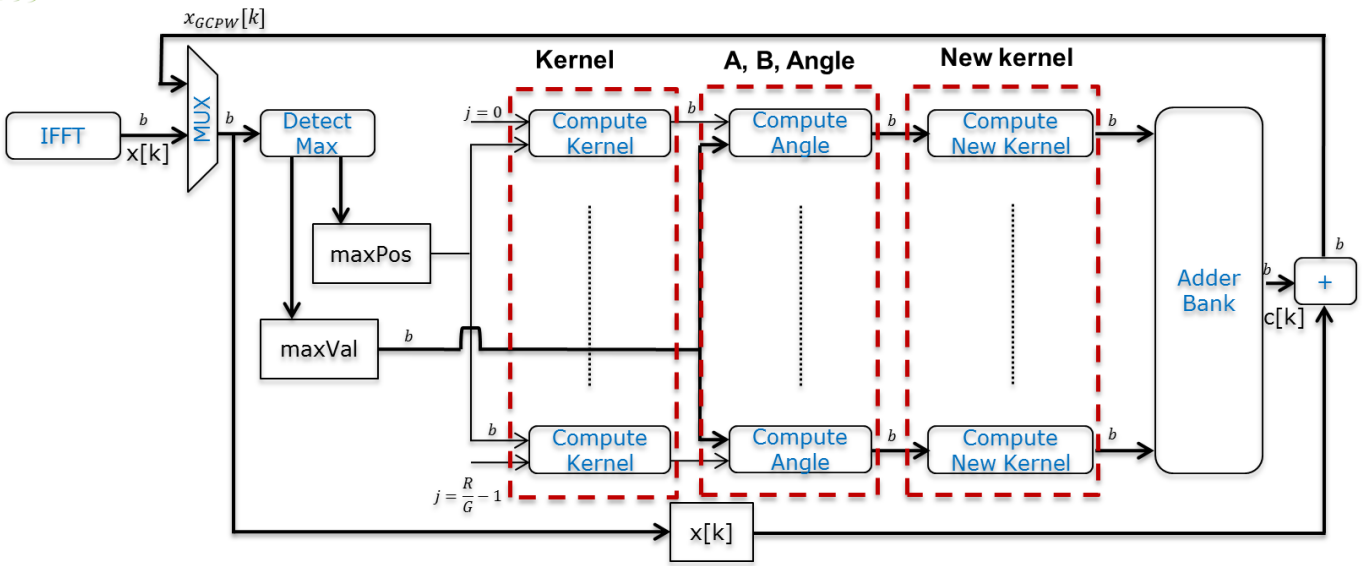

Fig. 3: Block diagram of GCPW algorithm.

At the i^{th} iteration, the block *Compute Kernel* calculates simultaneously the kernel values at the peak positions for each PRT within the group G_i as expressed below

$$c_j[maxPos(t)] = \frac{A_{max}}{N} e^{\jmath \frac{2\pi maxPos[t]\mathcal{P}_{i,j}}{N}}, \qquad (25)$$

with $1 + \frac{(i-1)R}{G} \leq j \leq 1 + \frac{iR}{G}$.

The kernel phases are then computed by the *Compute Angle* module as given in (Eq. 22). *A* and *B* represent the numerator and denominator of (Eq. 22), respectively.

The kernel generation for each PRT within the i^{th} group G_i is calculated by the *Compute New Kernel* module as

$$c_j[k] = \frac{A_{max}}{N} e^{-\jmath \Phi^*_{i,j}} e^{\jmath \frac{2\pi k \mathcal{P}_{i,j}}{N}}, \quad k \in [0, N-1]. \qquad (26)$$

The *Adder Bank* module generates the new kernel as

$$c[k] = \sum_{j \in G_i} c_j[k]. \qquad (27)$$

Finally, the signal is updated

$$x[k] = x[k] + c[k], \quad k \in [0, N-1]. \qquad (28)$$

Practically, the efficient implementation of GCPW algorithm requires the use of fixed-point architecture. Thus the signal at the output of each module of the GCPW block diagram should be quantized on b bits as illustrated in Fig. 3. Generally, the number of quantization bits required for each module should be minimized as long as the computation accuracy is maintained.

B. Overview of Fixed-Point Implementation and Quantization

Generally, efficient implementation of any digital signal processing algorithm in a communication system requires the use of fixed-point arithmetic. TR-based algorithms are usually designed and simulated using floating-point data types but they are finally implemented with fixed-point architectures with dedicated chips or Field Programmable Gate Array (FPGA). To represent a real number in computers (or any hardware in general), we can define a fixed-point number type simply by implicitly fixing the binary point to be at some position of a numeral. The fixed-point conversion process involves two main stages. The first stage defines the data binary point position through the determination of the integer part wordlength. This is achieved by evaluating data dynamic range in order to obtain the extreme values that have to be represented. Then, in the second stage, the data wordlengths are determined from the definition for each data of the fractional part wordlength. Thus, for a cost-effective implementation, the main goal is to minimize the data wordlength as long as the computation accuracy is maintained.

1) Fixed-point representation: A signed fixed-point data of wordlength b is made-up of a sign part represented by the most significant bit (MSB), an integer part represented by m bits and a fractional part represented by n bits as shown in Fig. 4, where $b = m + n + 1$. To define a fixed-point type conceptually, two parameters are needed, namely, wordlength and binary point position within the number. So, we denote fixed-point representation in a (b, n) format implying that total

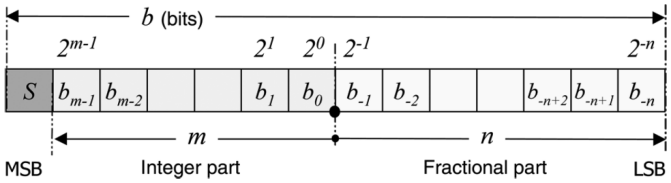

Fig. 4: A typical b-bit fixed-point representation of data.

wordlength is b and fractional part is n. This format implicitly implies that the integer part is $m = b - n - 1$. The value of a specific b-bit binary number in (b, n) format fixed-point representation is given by the expression

$$x = 2^{-n} \left[-2^{b-1} x_{b-1} + \sum_{i=0}^{b-2} 2^i x_i \right], \qquad (29)$$

where x_i represents the i^{th} bit of x. The resolution is the smallest non-zero magnitude representable. (b, n) format has resolution 2^{-n} and its range is given by $[2^b - 2^{-n}, -2^m]$.

2) Quantization: Conversion from floating-point to fixed-point can be viewed as a process of quantization, which maps input values from a large set to output values represented by a number of bits b. From cost and power consumption point of view, b must be kept as small as possible to the detriment of quantization and clipping noise. Considering an Analog to Digital Converter (ADC) with b bits and clipping levels $\pm A_{CL}$, the level of the Least Significant Bit (LSB) is $A_{LSB} = \frac{A_{CL}}{2^{b-1}}$. If the input samples are random, zero mean and uniformly distributed across the quantization levels over the full scale range of the ADC, the quantization error is uniform over $\left[\frac{-A_{LSB}}{2}, \frac{A_{LSB}}{2}\right]$. On the other hand, clipping noise is caused by the input samples dynamic range exceeding the clipping levels. When dealing with communication signals samples by an ADC, a trade-off exists between quantization and clipping noise: if the input signal is weakly amplified before the ADC, the quantization error is relatively high compared to no clipping noise. With strong amplified input signal, the ADC quantization error is small but more clipping occurs causing severe distortion. Hence, an optimum must be found to balance quantization and clipping noise. This is investigated more in details in next section.

C. MER Optimization by Trade-off between Quantization and Overflow Errors

Actually, optimal phase computation is the only module that requires high number of bits. It has been found that it is possible to perform this with fewer bits by scaling down A and B since the angle computation in (22) needs only their ratio. This scaling down can be achieved by simple shift register operations. It means that GCPW with an $\mathcal{O}(N)$ complexity has an inherent advantage in a fixed-point implementation with fewer bits, needing only some additional shift register operations.

VI. Simulation results

In this section, we evaluate the performance of the proposed GCPW algorithm in terms of MER vs IBO in both floating

and fixed point implementations.
In our simulations, we consider the HPA Rapp model with a knee factor $p = 6$ and $v_{sat} = 1$. We also consider ATSC 3.0 standard with 64 QAM constellation, $C_{red-coeff} = 0$, 8K and 32K modes. As previously mentioned in Section III-C-3, the number of active subcarriers is then equal to 8192 and 32768 respectively, in 8K and 32K modes while the number of PRTs is 72 and 288. The power boost for PAPR reduction is fixed at $\lambda = 10$ dB as specified by the ATSC 3.0 standard. Furthermore, the layer division multiplexing (LDM) mode of the ATSC 3.0 has not been activated in our simulations. Anyway, as LDM will not modify neither the time distribution of the signal nor the PRT positions, the same results would be obtained with LDM.

A. Performance Evaluation of Proposed TR-Based Algorithms

1) GICMP algorithm: The ATSC 3.0 standard specifies a minimum MER value of 27 dB at the transmitter to ensure sufficient signal quality within the designated coverage area [38]. We evaluate the MER of GICMP algorithm in 8K mode at IBO = 6.4 dB considering $S \in \{50, 80, 100, 200\}$, $G = \{4, 8, 12\}$ and 64 QAM. Results are summarized in Table II, where we can deduce that the best MER is obtained when $G = 12$ and $S = 80$.

TABLE II: MER at IBO = 6.4 dB for GICMP with: ATSC 3.0, 8K mode, 64 QAM and Rapp HPA model with $p = 6$.

	S=200	S=100	S=80	S=50
$G = 4$	33	33.28	33.33	33.24
$G = 8$	33.09	33.44	33.45	33.34
$G = 12$	33.01	33.35	33.48	33.32

The MER plot of GICMP with $S = 80$ and $G = \{4, 8, 12\}$ is shown in Fig. 5 and compared to ICMP with $S = 80$ and to the TTPC standard algorithm. Let us remind that this TTPC algorithm is the gradient-based TR algorithm including a power control scheme described in the last versions of the DVB-T2 and ATSC 3.0 standards. Furthermore, the performance of the optimal QCQP algorithm, which is not implementable as too complex, is given as reference. With only 4 groups, i.e, 4 iterations the GICMP algorithm outperforms the TTPC algorithm even after performing 30 iterations and is close to the ICMP algorithm. At IBO = 6.4 dB, GICMP (with $G = 4$) lags the optimal QCQP algorithm by merely 0.88 dB and offers 2.39 dB and 1.36 dB gain, respectively compared to the original signal and with TTPC. Moreover, the MER plot shows that GICMP with $S = 80$ and $G = 8$ (i.e, 8 iterations) is very close to the ICMP algorithm and to the QCQP algorithm (with a gap of 0.76 dB) and offers 2.51 dB and 1.48 dB gain, respectively compared to the original signal and with TTPC at IBO = 6.4 dB. Note that ICMP is expected to have better performance since the kernel obtained by activating one PRT at each iteration targets the reduction of multiple signal peaks. At each iteration, the kernel generation takes into consideration the optimization of the kernels computed at the previous iterations. However, the good performance is at

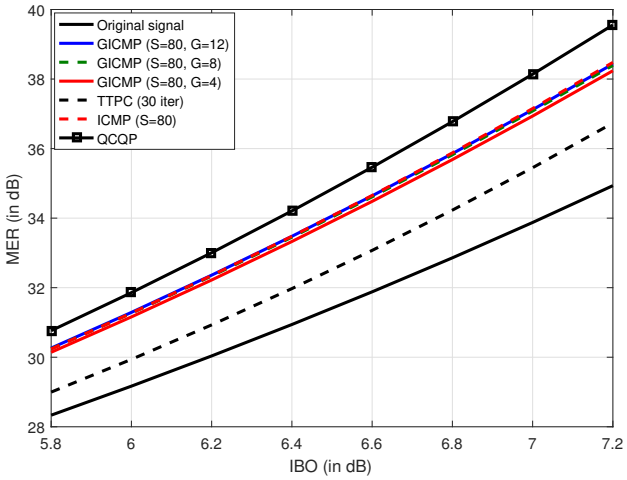

Fig. 5: MER with GICMP for: ATSC 3.0, 8K mode, 64 QAM and Rapp model HPA with $p = 6$.

the detriment of high number of iterations which equals the number of PRTs as mentioned in Section IV-B, which means 72 iterations in 8K mode. With GICMP, the kernel generation at each iteration is carried out for all the PRTs within the same group simultaneously. This lowers the total number of iterations which is now equal to the number of PRTs groups. Thus, GICMP with $G = 8$ offers almost identical performance with very low complexity and latency and is then more suited for implementation in ATSC 3.0 transmitters.

In 32K mode, we consider $S = \{100, 200\}$ and $G = \{8, 12\}$ and summarize the MER results at IBO = 6.4 dB in Table III.

TABLE III: MER at IBO = 6.4 dB for GICMP with: ATSC 3.0, 32K mode, 64 QAM and Rapp HPA model with $p = 6$.

	S=200	S=100
$G = 8$	33.21	33
$G = 12$	33.22	33.01

The MER plot is shown in Fig. 6 which confirms that the performances of GICMP with $G = 8$ and $G = 12$ are almost identical. Furthermore, the GICMP algorithm with only 8 iterations outperforms the TTPC algorithm which has very poor performance even after 30 executed iterations. At an IBO = 6.4 dB, GICMP with ($G = 8$, $S = 200$) offers 2.22 dB and 1.48 dB MER gain, respectively compared to the original signal and with TTPC. With $G = 8$, the MER of GICPM is almost identical to the ICMP algorithm while offering lower complexity with less latency since only 8 total iterations are needed instead of 288.

2) GCPW algorithm: With GCPW algorithm, maximum S first peaks above the threshold $\tilde{\lambda}$ are targeted in the PAPR reduction process. For every S peaks, there exists an optimal β value for GCPW algorithm that maximizes the MER, hence reducing the global latency without performance degradation compared to GICMP algorithm. The MER optimization is considered at an IBO operating point of 6.4 dB.

In Fig. 7, the optimal β value (see Eq. 24) is investigated in 8K mode considering $S = \{80, 100\}$ and $G\{8, 12\}$ groups. The MER of GICMP is independent of β and is shown as

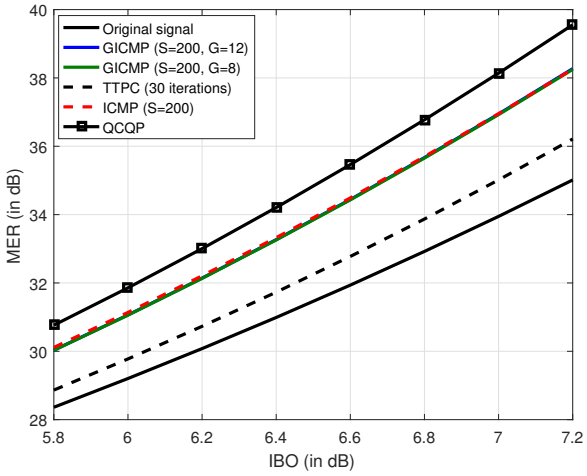

Fig. 6: MER with GICMP for: ATSC 3.0, 32K mode, 64 QAM and Rapp model HPA with $p = 6$.

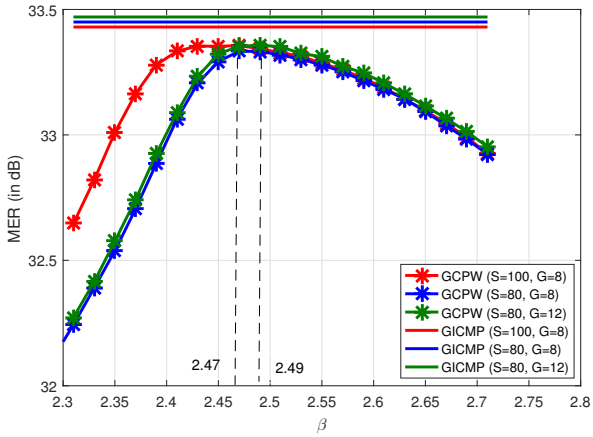

Fig. 7: MER vs. β, $S = \{80, 100\}$ $G = \{8, 12\}$ for: ATSC 3.0, 8K mode, Rapp HPA model with $p = 6$ and IBO = 6.4 dB.

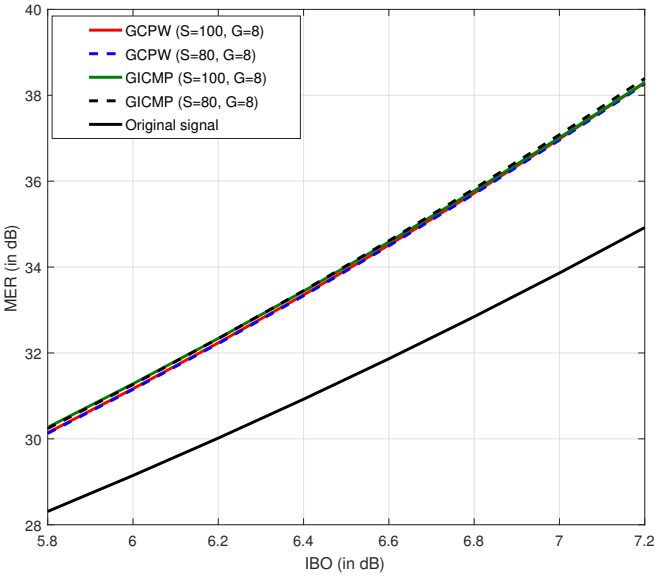

Fig. 8: MER with GCPW and GICMP ($G = 8$, $S = \{80, 100\}$) for: ATSC 3.0, 8K mode, 64 QAM and Rapp model HPA with $p = 6$.

reference. For $S = 80$, the optimal β value that maximizes the MER is 2.49. GCPW lags the GICMP algorithm by 0.12 dB and 0.11 dB when G equals 8 and 12, respectively. Therefore, increasing the number of groups does not improve the MER of GCPW. By increasing the number of peaks to $S = 100$ and setting $G = 8$, the gap between GICMP and GCPW algorithms is reduced to 0.08 dB and the MER is optimized when $\beta = 2.47$. In Fig. 8, we compare the MER performance of GCPW and GICMP algorithms with $G = 8$. At an IBO = 6.4 dB and $S = 80$, GCPW offers 33.33 dB MER, meaning that it outperforms the original signal by 2.41 dB and lags GICMP by 0.12 dB. By increasing S to 100, GCPW offers 33.35 dB MER, i.e, a gain of 2.43 dB compared to the original signal and a loss of merely 0.08 dB compared to GICMP. In this case, GCPW needs only storage of maximum $S = 100$ peak values while GICMP needs storage of all 8192 signal values in addition to a sorting operation. With this selected mode ($G = 8$, $S = 100$) almost identical MER results can be offered by GCPW with reduced complexity, latency and memory requirements compared to GICMP.

In Fig. 9, the optimal β value is investigated considering $S = \{100, 200\}$ in 32K mode with $G = \{8, 12\}$ groups. For $S = 100$ and $G = 12$, the MER is maximized for $\beta = 2.69$ but with a gap of 0.14 db compared to GICMP with $S = 100$ and $G = 12$. Hence, increasing the number of groups does not lead to any MER improvement. The number of targeted peaks is then increased to $S = 200$. In this case, the optimal β is 2.57 but the maximum MER obtained with $G = 8$ lags the GICMP MER by 0.05 dB. By increasing the number of groups G to 12, the MER gap between GCPW and GICPM is merely 0.01 dB. GCPW offers an MER of 33.21 dB at an IBO operating point of 6.4 dB, meaning almost identical performance as GICMP while reducing the global latency. Indeed, GCPW needs only storage of maximum $S = 200$ absolute peaks while GICMP needs storage of all 32768 absolute samples in addition to a sorting operation. In Fig. 10, we compare the MER performance of the proposed algorithm with GICMP and the original signal. We consider $G = 12$, $S = 200$ and $\beta = 2.57$ for GICMP and GCPW configurations. As we can notice, the MER curves of GICMP and GCPW are identical. Indeed, at 6.4 dB IBO, GCPW offers 33.21 dB MER meaning that it outperforms the original signal by 2.32 dB and lags GICMP by only 0.01 dB. Hence, with this selected mode ($G = 12$, $S = 200$) the new TR-based GCPW algorithm offers very good performance and complexity/latency/memory requirements trade-off for the ATSC 3.0 standard even for 32K mode.

B. Performance Evaluation of GCPW Algorithm in Fixed-Point Architecture

1) Quantization optimization: As stated earlier, the input samples amplitude must be modified to fit into the ADC dynamic range so as the quantization and clipping noises are balanced. In this section, we investigate the configuration of an ADC quantifying the input samples on 12 and 16 bits

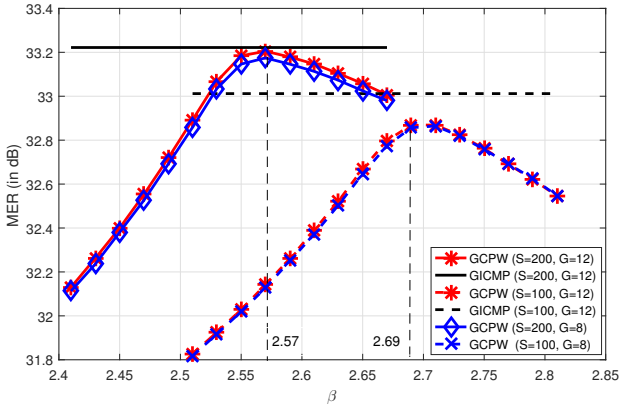

Fig. 9: MER vs. β, $S = \{100, 200\}$ $G = \{8, 12\}$ for: ATSC 3.0, 32K mode, Rapp HPA model with $p = 6$ and IBO = 6.4 dB.

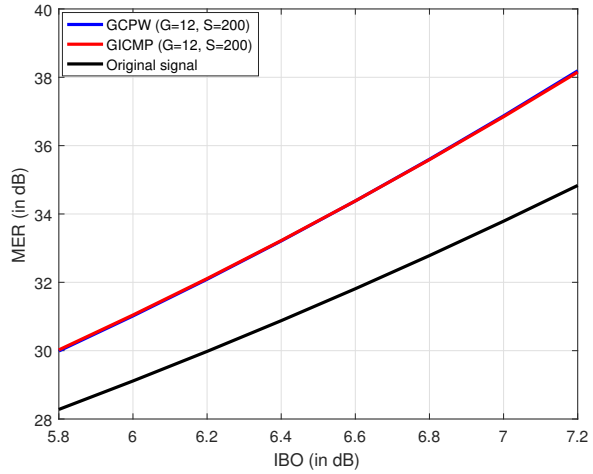

Fig. 10: MER with GCPW and GICMP ($G = 12$, $S = 200$) for: ATSC 3.0, 32K mode, 64 QAM and Rapp model HPA with $p = 6$.

with clipping levels equal to $\pm A_{CL}$. Independently of any PAPR reduction algorithm, we consider the OFDM time-domain complex signal at the IFFT output (see Eq. 1). It is well known that when the number of subcarriers is high, the real and the imaginary parts of the OFDM signal, which are quantized separately, are Gaussian distributed. In Fig. 11, we illustrate for both 12 and 16 bits quantization the MER and the percentage of clipped samples when varying the ratio between the standard deviation σ of the input signal and the clipping level A_{CL} with

$$A_{CL} = \alpha\sigma. \tag{30}$$

Solid and dash lines correspond to 12 and 16 bits quantization, respectively. There exists an optimum value of α that globally minimizes the clipping noise and the quantization noise leading to the maximum MER value. Since the MER metric is the considered figure of merit in this paper, it is of great interest to find this optimum value. From Fig. 11, we can deduce that MER is maximized when $\alpha = 4.8$ and $\alpha = 5.18$ for 12 and

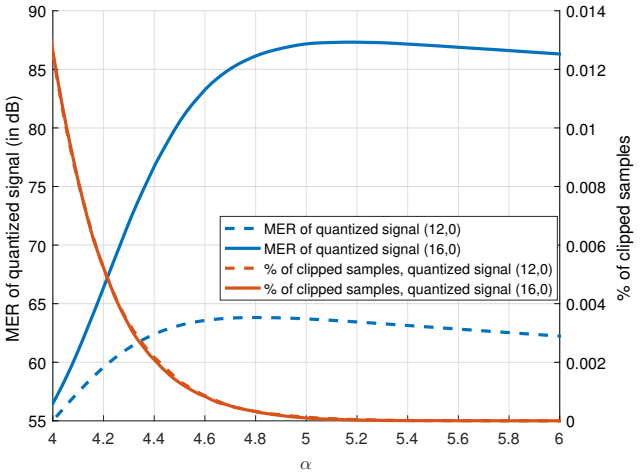

Fig. 11: MER vs α for: ATSC 3.0, 32K mode, (12, 0) and (16, 0) signal quantization.

16 bits quantization, respectively. We summarize in Table IV the obtained MER and clipping percentage for optimum α. As expected, in case of 16 bits quantization the maximum MER value is better than with 12 bits with a difference slightly lower than 24 dB corresponding to the well known rule of 6 dB per bit. Furthermore, for 16 bits quantization, the optimum value of α is higher leading to a lower number of clipped samples.

TABLE IV: MER and clipping percentage of optimized 12 and 16 bit quantization.

b	α	MER (in dB)	Clipping %
12 bits	4.8	63.82	3.13 10^{-4}
16 bits	5.18	87.32	3.48 10^{-5}

2) Choice of GCPW quantization parameters: We consider the GCPW block diagram depicted in Fig. 3 and the quantization of the OFDM time-domain signal $x[k]$ at the IFFT output on (12, 0) and (16, 0) bits. The GCPW is evaluated in three scenarios: (16, 4), (16, 0) and (20, 4) bits quantization and for 8K and 32K modes. It has been found that in fixed-point the GCPW algorithm needs at least 16 bits to represent the signal at each block. Hence, quantized original signal on (12, 0) bits is compared to GCPW on (16, 4) bits, meaning that the integer and fractional parts are represented by 12 and 4 bits, respectively. Thus, the optimal σ value for both the original signal and with GCPW is $\sigma = \frac{A_{CL}^{12}}{4.8}$, with A_{CL}^{12} the clipping level of (12, 0) quantization. Similarly, the original signal quantized on (16, 0) bits is compared to quantized GCPW on both (16, 0) and (20, 4) bits. In the second case, 4 bits are dedicated to the fractional part while keeping the same optimal σ value which is equal to $\frac{A_{CL}^{16}}{5.18}$, with A_{CL}^{16} the clipping level of (16, 0) quantization.

3) Performance evaluation of quantized GCPW in 8K mode: Taking into account the MER value at an IBO operating point of 6.4 dB, we search the quantization format (b, n) for each block *Kernel*, *A*, *B*, *Angle* and *New Kernel* so as the loss compared to the floating-point is minimized. As mentioned

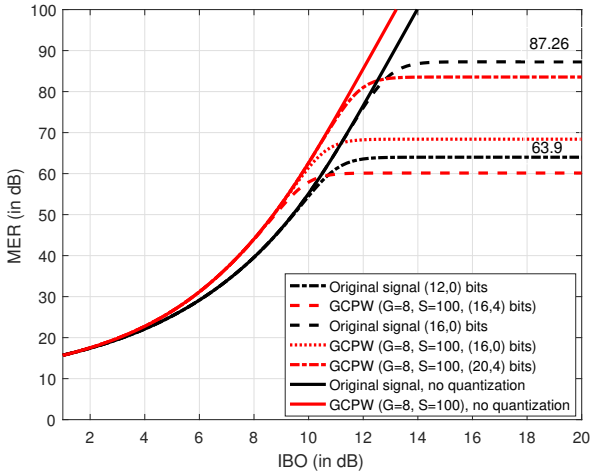

Fig. 12: MER of original signal and with GCPW with/without quantization for: ATSC 3.0, 8K mode, 64 QAM and Rapp model HPA with $p = 6$.

earlier, A and B are scaled down by the same factor since only their ratio is needed for angle computation. Table V summarizes the quantization parameters for 8K mode.

The MER plot in 8K mode is shown in Fig. 12 where

TABLE V: Quantization parameters (b, n) for each GCPW block in 8K mode.

$x[k]$	x_{GCPW}	*Kernel*	*A*	*B*	*Angle*	*New Kernel*
(12,0)	(16,4)	(16,9)	(16,3) $2^{-13\dagger}$	(16,3) $2^{-13\dagger}$	(16,12)	(16,9)
(16,0)	(16,0)	(16,6)	(16,3) $2^{-15\dagger}$	(16,3) $2^{-15\dagger}$	(16,10)	(16,6)
	(20,4)	(20,10)	(20,3) $2^{-15\dagger}$	(20,3) $2^{-15\dagger}$	(20,12)	(20,10)

† *A* and *B* are scaled by the same factor.

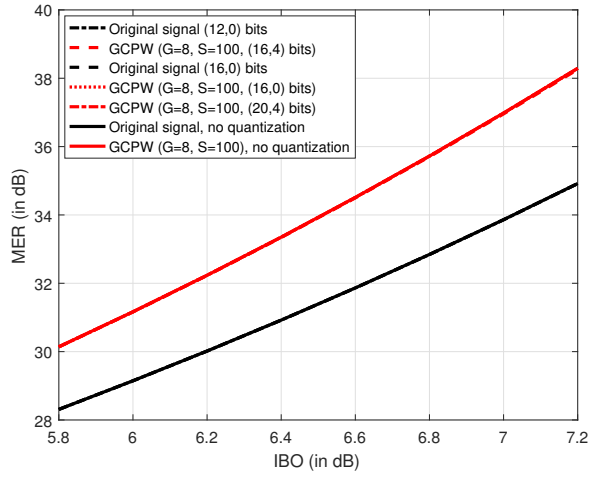

Fig. 13: MER of original signal and with GCPW with/without quantization for: ATSC 3.0, 8K mode, 64 QAM and Rapp model HPA with $p = 6$.

black and red curves correspond to the original signal and with GCPW, respectively. Fig. 13 focuses on the IBO interval [5.8 dB, 7.2 dB] where the 4 red curves corresponding to the GCPW algorithm are identical and the 3 black curves corresponding to the original signal are also identical. For both signals, quantization does not degrade MER performance at the IBO operating point of 6.4 dB. Moreover, the MER gain of quantized GCPW compared to quantized original signal remains 2.43 dB at IBO = 6.4 dB. In fixed-point, we notice that MER no longer increases with IBO but saturates after a certain IBO value. As shown in Fig. 12, the MER of original quantized signal saturates at 63.9 dB and 87.26 dB for (12, 0) and (16, 0) quantization, respectively. As expected, the difference between the two MER saturation values is slightly lower than 24 dB corresponding to the difference of 4 bits. Concerning quantized signal with GCPW, we notice that MER saturates at values which are slightly lower than with original signal. This is due to the several blocks within GCPW algorithm such as *Kernel* and *Angle* that are more prone to quantization effects. Additionally, we notice that by dedicating more bits to GCPW modules, the maximal MER values are improved as well as the IBO operating interval. In fact, we define the MER gain illustrated in Fig. 14 as

$$MER_{gain} = MER_{GCPW} - MER_{Original}, \tag{31}$$

where, MER_{GCPW} and $MER_{Original}$ are extracted from Fig. 12 with and without quantization. We can notice that the MER gain increases with IBO until a maximum value. Comparing quantized GCPW on (16, 4) bits to the original quantized signal on (12, 0) bits, the maximum MER gain offered by GCPW is 5.29 dB at IBO = 9 dB. If we target an MER gain higher than 2 dB, which is already considered as a significant gain, the IBO operating interval is then [6 dB, 10.3 dB]. In case of (16, 0) bits quantization, GCPW offers a maximum MER gain of 6.44 dB at IBO = 9.8 dB and an operating IBO interval [6 dB, 10.9 dB]. By allowing more bits to the GCPW modules (i.e (20, 4) bits), a maximum MER gain of 8 dB can be obtained at IBO = 10.8 dB with wider IBO operating interval [6 dB, 12.5 dB].

4) Performance evaluation of quantized GCPW in 32K mode: Again, the quantization format (b, n) for each block of the GCPW algorithm, so as the loss compared to the floating-point is minimized at IBO = 6.4 dB, is searched. Table VI summarizes the quantization parameters in 32K mode.

TABLE VI: Quantization parameters (b, n) for each GCPW block in 32K mode.

$x[k]$	x_{GCPW}	*Kernel*	*A*	*B*	*Angle*	*New Kernel*
(12,0)	(16,4)	(16,11)	(16,3) $2^{-13\dagger}$	(16,3) $2^{-13\dagger}$	(16,12)	(16,11)
(16,0)	(16,0)	(16,7)	(16,3) $2^{-15\dagger}$	(16,3) $2^{-15\dagger}$	(16,10)	(16,7)
	(20,4)	(20,11)	(20,3) $2^{-15\dagger}$	(20,3) $2^{-15\dagger}$	(20,12)	(20,11)

† *A* and *B* are scaled by the same factor.

The MER plot in 32K mode is shown in Fig. 15 where black and red curves correspond to the original signal and with GCPW, respectively. Fig. 16 focuses on the IBO interval

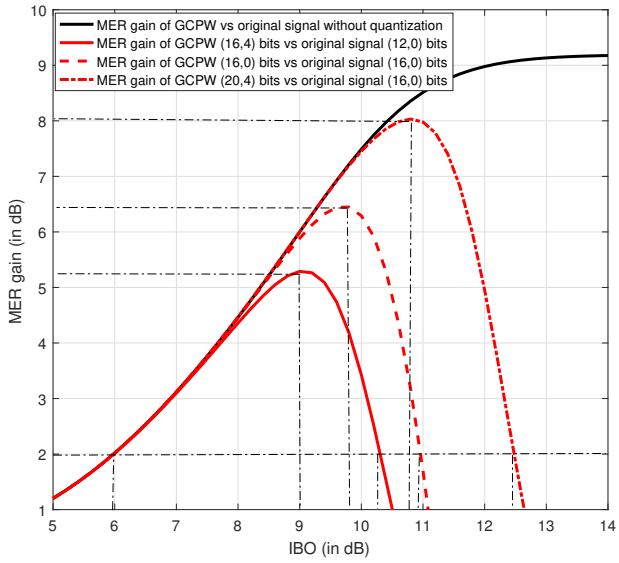

Fig. 14: MER gain of GCPW with/without quantization for: ATSC 3.0, 8K mode, 64 QAM and Rapp model HPA with $p = 6$.

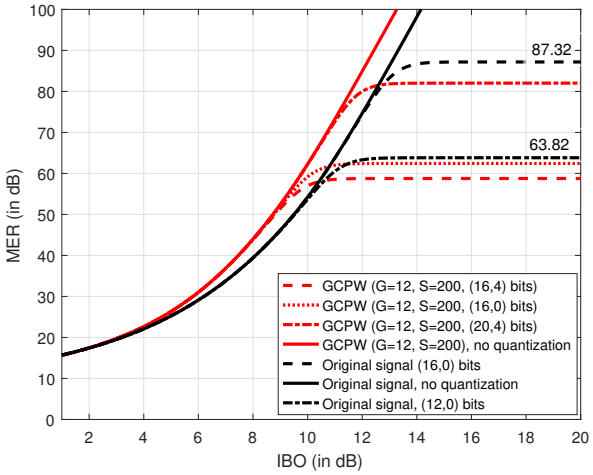

Fig. 15: MER of original signal and with GCPW with/without quantization for: ATSC 3.0, 32K mode, 64 QAM and Rapp model HPA with $p = 6$.

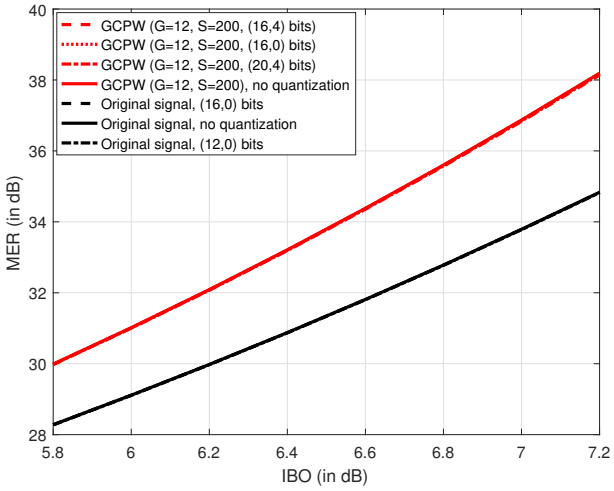

Fig. 16: MER of original signal and with GCPW with/without quantization for: ATSC 3.0, 32K mode, 64 QAM and Rapp model HPA with $p = 6$.

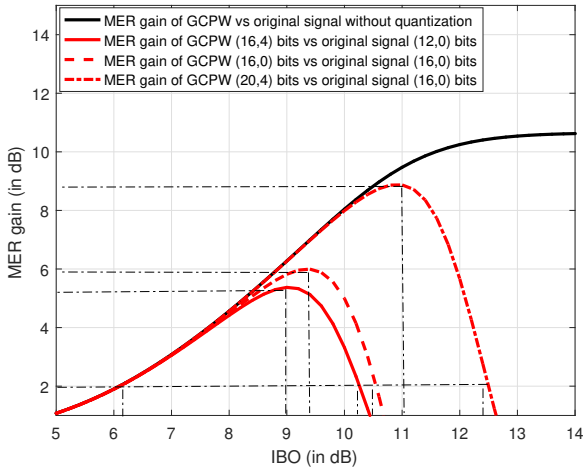

Fig. 17: MER gain of GCPW with/without quantization for: ATSC 3.0, 32K mode, 64 QAM and Rapp model HPA with $p = 6$.

[5.8 dB, 7.2 dB] where the 4 red curves corresponding to the GCPW algorithm are identical and the 3 black curves corresponding to the original signal are also identical. Again, for both signals, quantization does not degrade the MER performance at the IBO operating point of 6.4 dB. Indeed, the MER gain of quantized GCPW compared to quantized original signal remains 2.32 dB at IBO = 6.4 dB. In 32K also, we notice that the MER in fixed-point no longer increases with IBO but saturates after a certain value. As shown in Fig. 15, the MER of original quantized signal saturates at 63.82 dB and 87.18 dB for (12, 0) and (16, 0) quantization, respectively. As in 8K mode, we notice that the MER of quantized GCPW saturates at lower values compared to the original signal. Additionally, the MER of quantized GCPW saturates at lower values than in 8K mode since in this mode only $G = 8$ and $S = 100$ are considered instead of $G = 12$ and $S = 200$ in 32K mode for GCPW computations. This means that GCPW is less impacted by the accumulation of quantization error in 8K mode than in 32K mode. Moreover, we notice that by dedicating more bits to GCPW modules, the maximal MER values are improved as well as the IBO operating interval. The MER gain (see Eq. 31) is illustrated in Fig. 17. Comparing original signal quantized on (12, 0) with GCPW algorithm on (16, 4) bits, the maximum MER gain is 5.37 dB at IBO = 9 dB. If an MER gain higher than 2 dB is targeted, the IBO operating interval is then [6.2 dB, 10.2 dB]. With (16, 0) bits quantization, GCPW offers a maximum MER gain of 5.9 dB at IBO = 9.4 dB and an operating IBO interval [6.2 dB, 10.4 dB]. By dedicating more bits to the GCPW modules (i.e (20, 4) bits), a maximum MER gain of 8.87 dB can be obtained at IBO = 11 dB with a wider IBO operating interval of [6.2 dB, 12.4 dB].

5) Synthesis of the performance: We synthesize the MER gain of quantized GCPW algorithm compared to quantized

original signal in 8K and 32K modes. Table VII summarizes the MER gain at IBO values of 6.4 dB and 9 dB considering (16, 4), (16, 0) and (20, 4) quantization. First, at an IBO operating point of 6.4 dB the MER gain is unchanged compared to floating-point and is equal to 2.43 dB and to 2.32 dB in 8K and 32K, respectively. This means that quantization does not impact the proposed GCPW algorithm at the IBO operating point and a considerable gain can still be offered. Second, an MER gain up to 8 dB and to 9 dB can be achieved at IBO = 10.8 dB and at IBO = 9 dB, respectively in 8K and 32K mode with (20, 4) quantization. Finally, an MER gain higher than 2 dB in 8K mode can be obtained within an IBO operating interval of [6 dB, 10.3 dB] for (16, 4) quantization and within [6 dB, 12.5 dB] for (20, 4) quantization. In 32K mode, the IBO operating intervals for an MER gain higher than 2 dB are within [6.2 dB, 10.2 dB] for (16, 4) quantization and within [6.2 dB, 12.4 dB] for (20, 4) quantization.

TABLE VII: MER gain of GCPW vs original signal with quantization for: ATSC 3.0, 8K and 32K modes, 64 QAM and Rapp model HPA with $p = 6$.

IBO (dB)	8K mode			32K mode		
	(16,4)	(16,0)	(20,4)	(16,4)	(16,0)	(20,4)
6.4	2.43	2.43	2.43	2.32	2.32	2.32
9	5.29	5.88	6	5.37	5.82	6.26

VII. Conclusion

This paper deals with the PAPR issue in the ATSC 3.0 standard. As for any multicarrier communication system, the OFDM time-domain signal at the ATSC 3.0 transmitters may have very high peak values which can be severely distorted by the HPA. Due to these severe fluctuations, the HPA operating point should be backed off from its NL region which leads to very poor power efficiency. To overcome this issue, PAPR reduction algorithms are unavoidable. In this paper, we present a novel TR-based algorithm named as Grouped Carrier Peak Windowing (GCPW) implementable and compatible with the ATSC3.0 standard. The proposed algorithm is based on a new definition of the PAPR reducing signal. Differently from the gradient-based standard algorithm proposed in the ATSC 3.0 standard, the proposed kernel is easily computed with no need of additional IFFT operations or power control and benefits from all the power dedicated to PAPR reduction purposes.

This algorithm divides the available PRTs into G groups and sets the total number of iterations to G. Each kernel targets the cancellation of maximum S highest signal peaks. To select the S highest peaks, the whole OFDM time-domain samples should be stored and then sorted, leading to high latency and memory resources. Taking into account the different issues related to the implementation such as latency, complexity and memory resources requirements, we proposed a novel method to detect the targeted peaks. Indeed, only the first set $\mathcal{S}$ of peaks higher than a predefined threshold are processed by the GCPW algorithm. The optimization of this threshold is detailed in this paper. The performance of GCPW in terms of MER is evaluated in 8K and 32K modes which are the preferred modes for mobile and fixed reception, respectively. In both modes, the GCPW parameters are optimized taking into account the GCPW MER. The selected parameters are $(G = 8, \quad S = 100)$ and $(G = 12, \quad S = 200)$ for 8K and 32K, respectively, meaning that only maximum $S = 100$ (respectively $S = 200$) peaks are stored instead of 8192 samples in 8K mode (respectively 32768 in 32K mode).

We showed through simulations, that the novel algorithm offers very good performance/complexity/latency/memory resources trade-off. The MER performances of the GCPW algorithm highly outperforms those of the gradient-based standard algorithm while only necessitating 8 and 12 total iterations in 8K and 32K modes, respectively. At the IBO operating point of 6.4 dB, a significant MER gain of 2.43 dB and 2.32 dB is achieved in 8K and 32K modes, respectively. Furthermore, the performances of this GCPW algorithm are very close to those of the optimal QCQP algorithm which is too complex to be implemented.

Generally, TR-based algorithms are designed in floating-point but are finally implemented in fixed-point with dedicated chips or FPGA. Therefore, we presented an in-depth study of the implementation of the novel GCPW algorithm in fixed-point architecture. The quantization of the signal at the different blocks related to the GCPW algorithm has been optimized in order to minimize the MER loss compared to floating-point. Again, quantized GCPW is evaluated with ATSC 3.0 standard in both 8K and 32K modes. Simulation results show that the quantization does not impact the MER gain at the IBO operating point. Furthermore, different IBO operating intervals and MER gains can be obtained according to the chosen quantization.

To conclude, this study has shown that the GCPW TR-based algorithm is a very efficient and implementable candidate for ATSC3.0 standard transmitters.

Acknowledgment

This work has received a French state support granted to both the Convergence TV project through the 20^{rd} FUI (transverse inter-ministry funding) program and the GreenTEA project through the Eurostars/EUREKA program of the European Commission. The authors would also like to thank the "Image & Réseaux" and "Cap Digital" French business clusters for their support of this work.

References

[1] S. H. Han, and J. H. Lee, "An overview of peak-to-average power ratio reduction techniques for multicarrier transmission," *IEEE Trans. Wireless Communications*, vol. 12, no. 2, pp. 56-65, Apr. 2005.

[2] O. E. M. J. F.-G. Garcia, and J. M. Pacz-Borallo, "Peak Power Reduction for OFDM Systems With Orthogonal Pilot Sequences," *IEEE Trans. Wireless Communications*, vol. 5, no. 1, pp. 1536-1276, Jan. 2006.

[3] T. Jiang, and Y. Wu, "An overview: Peak-to-Average Power Ratio Reduction Techniques for OFDM systems," *IEEE Trans. on Broadcasting*, vol. 54, Issue, 2, pp. 257-268, June, 2008.

[4] G. Wunder, R. F. H. Fischer, H. Boche, S. Litsyn and J. No "The PAPR Problem in OFDM Transmission: New Directions for a Long-Lasting Problem," *EEE Signal Processing Magazine*, Vol. 30, No. 6, pp. 130-144, 2013.

[5] X. Li, and L. J. Cimini, "Effects of clipping and filtering on the performance of OFDM," IEEE Communication Letters, vol. 2, no. 5, pp. 131-133, May 1998.

[6] T. A. Wilkinson, and A. E. Jones, "Minimization of the peak-to-mean envelope power ratio of multi-carrier transmission schemes by block coding," *IEEE VTC*, vol. 2, pp. 825-829, Chicago, Jul. 1995.

[7] S. H. Muller, and J. B. Huber, "OFDM with reduction peak to average power ratio by optimum combination of partial transmit sequences," *IEEE Electronics Letters*, vol. 33, pp. 368-369, Feb. 1997.

[8] R. W. Bauml, R. F. H. Fischer, and J. B. Huber, "Reducing the peak-to-average power ratio of multi-carrier modulation by selected mapping," *IEEE Electronics Letters*, vol. 32, no. 22, pp. 2056-2057, Oct. 1996.

[9] J. Tellado, "Peak to Average Ratio Reduction for Multi-carrier Modulation," *Ph.D. Thesis*, Stanford University, Stanford, CA, USA, 1999.

[10] B. S. Krongold, and D. L. Jones, "PAR reduction in OFDM via active constellation extension," *IEEE Trans. Broadcasting*, vol. 49, pp. 258-268, Sep. 2003.

[11] ETSI, "Frame structure channel coding and modulation for a second generation digital terrestrial television broadcasting system (DVB-T2)," *ETSI EN 302755 V1.1.1*, Sep. 2009.

[12] ATSC 3.0, "ATSC Proposed Standard: Physical Layer Protocol," 2016.

[13] Y. Wang, W. Chen, and C. Tellambura, "Genetic Algorithm Based Nearly Optimal Peak Reduction Tone Set Selection for Adaptive Amplitude Clipping PAPR Reduction," *IEEE Trans. Broadcasting*, vol. 58, Issue: 3 pp. 462-471, Sept. 2012.

[14] J.-C. Chen, M.-H. Chiu, Y.-S. Yang and C.-P. Li, "A Suboptimal Tone Reservation Algorithm Based on Cross-Entropy Method for PAPR Reduction in OFDM Systems," *IEEE Trans. Broadcasting*, vol. 57, No. 3 pp. 752-756, Sep. 2011.

[15] J.-C. Chen, and C.-P. Li,"Tone Reservation Using Near-Optimal Peak Reduction Tone Set Selection Algorithm for PAPR Reduction in OFDM Systems," *IEEE Signal Processing Letters*, vol. 17, pp. 933-936, Nov., 2010.

[16] D.-W. Lim, H.-S. Noh, H.-B. Jeon, J.-S. No, and D.-J. Shin, "Multi-Stage TR Scheme for PAPR Reduction in OFDM Signals," *IEEE Trans. Broadcasting*, vol. 55, No. 2 pp. 300-304, June, 2009.

[17] Y. Z. Jiao, X. J. Liu, and X. A. Wang, "A Novel Tone Reservation Scheme with Fast Convergence for PAPR Reduction in OFDM Systems," *IEEE Consumer Communications and Networking Conference (CCNC)*, Las Vegas, NV, USA, Jan, 2008.

[18] H. Li, T. Jiang, and Y. Zhou,"An Improved Tone Reservation Scheme With Fast Convergence for PAPR Reduction in OFDM Systems," *IEEE Transactions on Broadcasting*, vol. 57, No. 4, pp. 902-906, Dec., 2011.

[19] T. Jiang, C. Ni, C. Xu, and Q. Qi, "Curve Fitting Based Tone Reservation Method with Low Complexity for PAPR Reduction in OFDM Systems," *IEEE Communications Letters*, vol. 18, no. 5, pp. 805-808, Apr. 2014.

[20] S. Rosati, E. A. Candreva, and G. E. Corazza, "Rotation Invariant Subcarrier Mapping over DVB-T2 Reserved Tones," *IEEE Vehicular Technology Conference (VTC Spring)*, pp. 1-5, Jun. 2013.

[21] F. Tosato, M. Sandell, and M. Tanahashi, "Tone reservation for PAPR reduction: An optimal approach through sphere encoding," *IEEE International Conference on Communications*, pp. 1-6, May 2017.

[22] M. L. Diallo, M. Chafii, J. Palicot, and F. Bader, "Modified Tone Reservation for PAPR Reduction in OFDM Systems," *European Signal Processing Conference (EUSIPCO)*, Budapest, Hungary, Sept. 2016.

[23] J. Bai, Y. Li, W. Cheng, *et. al*, "A Novel Peak-To-Average Power Ratio Reduction Scheme via Tone Reservation in OFDM Systems," *China Communications*, vol. 14, No. 11, pp. 279-290, Dec. 2017.

[24] P. Y. Yu, and S.B. Jin. A Low Complexity Tone Reservation Scheme Based on Time-Domain Kernel Matrix for PAPR Reduction in OFDM Systems, *IEEE Transactions on Broadcasting,* vol. 61, No. 4, pp 710-716, 2015

[25] Y. J. Wang, S. Xie, Z.B. Xie. FISTA-based PAPR Reduction Method for Tone Reservations OFDM Systems , *IEEE Wireless Commun. Lett.*, Vol. 7, No. 3, pp. 300-303, 2018

[26] K. C. Bulusu, M. Crussière, J.-F. Hélard, R. Mounzer, Y. Nasser, O. Rousset, and A. Untersee "Quasi-Optimal Tone Reservation PAPR Reduction Algorithm for Next Generation Broadcasting Systems: A Performance/Complexity/Latency Tradeoff With Testbed Implementation," *IEEE Trans. on Broadcasting*, "DOI:10.1109/TBC.2018.2811623", pp. 1-7, March 2018.

[27] C. Rapp, "Effects of HPA nonlinearity on 4-DPSK-OFDM signal for digital sound broadcasting systems," *European Conference on Satellite Communications*, pp. 22-24, Liège, Belgium, Oct.1991.

[28] R. Van Nee, and R. Prasad, *OFDM for Wireless Multimedia Communications*, Artech House, Boston, Mass., USA, 2000.

[29] J. Tellado, and J. Cioffi, "Peak power reduction for multicarrier transmission," *IEEE CTMC, GLOBECOM*, Sydney, Australia, Nov. 1998.

[30] S. Zabre, J. Palicot, Y. Louet, and C. Lereau "SOCP approach for OFDM Peak-to-Average Power Ratio reduction in the signal adding context," *IEEE International Symposium on Signal Processing and Information Technology*, Vancouver, BC, Canada, Aug. 2006.

[31] S. Janaaththanan, C. Kasparis, and Barry G. Evans "A gradient based algorithm for PAPR reduction of OFDM using Tone Reservation technique," *IEEE Vehicular Technology Conference*, Singapore, Singapore, May. 2008.

[32] R. Mounzer, Y. Nasser , M. Crussière, and J.-F. Hélard "Power control optimization for tone reservation based PAPR reduction algorithms," *IEEE International Symposium on Personal, Indoor, and Mobile Radio Communication* , Washington, DC, USA, Sept. 2014.

[33] K. C. Bulusu, M. Crussière, J.-F. Hélard, R. Mounzer, and Y. Nasser, "A Low Latency Algorithm for Efficient PAPR Reduction for DVB-T2 and ATSC 3.0 Broadcast," *IEEE International Symposium on Broadband Multimedia Systems and Broadcasting*, Cagliari, Italy, Jun. 2017.

[34] R. Mounzer, M. Crussière, Y. Nasser, and J.-F. Hélard, "Tone reservation based PAPR reduction technique with individual carrier power allocation for multiple peaks reduction," *Proceedings of IEEE Vehicular Technology Conference VTC-Spring*, Glasgow, Scotland, May 2015.

[35] M. Mroué, A. Nafkha, J. Palicot, B. Gavalda, and N. Dagorne, "Performance and Implementation Evaluation of TR PAPR Reduction Methods for DVB-T2," *International Journal of Digital Multimedia Broadcasting*, vol. 2010, Aug. 2010.

[36] M. Mroué, A. Nafkha, and J. Palicot, "An innovative low complexity PAPR reduction TR-based technique for DVB-T2 system," *International Congress on Ultra Modern Telecommunications and Control Systems and Workshops*, Moscow, Russia, Oct. 2010.

[37] ETSI, "Digital Video Broadcasting (DVB); Frame structure channel coding and modulation for a second generation digital terrestrial television broadcasting system (DVB-T2)," *ETSI EN 302 755 V1.3.1*, Sep. 2011.

[38] ATSC 3.0, "ATSC Recommended Practice: Transmission Measurement and Compliance for Digital Television," 2014.

Naila Lahbabi received her master degrees in advanced systems in radio communications from Supelec, France in 2012. In 2017, she obtained her Ph.D. degrees in Sciences and Technologies of Information and Communication from IMT Atlantique and Orange Labs, France. During her Ph.D., she worked on algorithms for transmission and reception in multicarrier communication systems signaling faster than the Nyquist rate. Currently, she is pursuing her post-doctorate at the National Institute of Applied Sciences (INSA). She is the author of technical papers in 3 international conferences and holds 3 patents. Her research interests include digital communication, new waveforms and PAPR reduction techniques.

S. S. Krishna Chaitanya Bulusu (M15) received the B.Tech. degree in electronics and communications engineering from Pondicherry Engineering College, Pondicherry, India, in 2005, the M.S. degree in mobile communications from Tlcom ParisTech/Institute Eurecom, Sophia Antipolis, France, in 2009, and the Ph.D. degree in radiocommunications from Conservatoire National des Arts et Mtiers, Paris, France, in 2016. From 2016 to 2017, he was a Post-Doctorant with the National Institute of Applied Sciences, Rennes, France. Since 2018, he has been an Assistant Professor affiliated to the Mahindra cole Centrale, Hyderabad. His research interests include digital signal processing, digital communications, embedded systems, massive MIMO, post-OFDM waveforms with special focus on HPA linearization, PAPR reduction, channel estimation, and receiver synchronization techniques. He has authored technical papers in eight international conferences and three international journals, and holds a French patent. He has been involved in few European and French research projects involving broadcasting systems and PMR systems. He was a recipient of the Thales-French Ministry of External Affairs Scholarship in 2007. He is a member of the Institution of Engineers (India).

Jean-François Hélard received his Dipl.-Ing. and his Ph.D in electronics and signal processing from the National Institute of Applied Sciences (INSA) in Rennes in 1981 and 1992 respectively. From 1982 to 1997, he was research engineer and then head of channel coding for the digital broadcasting research group at France Telecom Research Center in Rennes. In 1997, he joined INSA Rennes, which is one of the "Grandes Ecoles" in France, where he is today full-time professor of classe exceptionelle, which is the highest rank. He was Director of Research of INSA Rennes during 3 years from 2010 to 2013. He was also during 8 years Deputy Director of the Rennes Institute for Electronics and Telecommunications (IETR, UMR CNRS 6164), which is an academic research laboratory of 400 people, created in 2002 in association with the CNRS. His research interests lie in signal processing techniques for digital communications, such as space-time and channel coding, multicarrier modulation, as well as multi-user communications and cross-layer techniques. He is involved in several European and national research projects in the fields of digital video terrestrial broadcasting, mobile radio communications and cellular networks, power-line and ultra-wide-band communications, cooperative communications and relaying techniques. He is a senior member of IEEE, author and co-author of more than 270 technical papers in international scientific journals and conferences, and holds 15 European patents.

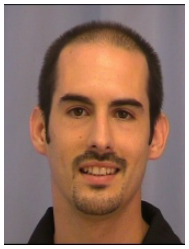

Matthieu Crussière received the M.Sc. and Ph.D. degrees in electrical engineering from the National Institute of Applied Sciences (INSA), France, in 2002 and 2005, respectively. Since 2005, he has been an associate professor affiliated to the Research Institute of Electronics and Telecommunications (IETR) of Rennes, France. In addition, in 2014, he started collaborations as an associate researcher at the Institute of Research and Technology (IRT) B-COM in Rennes. His main research interests lie in digital communications and signal processing, with a particular focus on multicarrier and multiantenna systems. He is a member of IEEE and is author or co-author of more than 120 technical papers in international conferences and journals. He has been involved in several European and French national research projects in the field of powerline, broadcasting, ultra wideband, and mobile radio communications.